

A projection method to extract biological membrane models from 3D material models

Farshad Roohbakhshan, Thang X. Duong, and Roger A. Sauer ¹

Aachen Institute for Advanced Study in Computational Engineering Science (AICES), RWTH Aachen University, Templergraben 55, 52056 Aachen, Germany

Published² in *The Journal of the Mechanical Behavior of Biomedical Materials*,

DOI: [10.1016/j.jmbbm.2015.09.001](https://doi.org/10.1016/j.jmbbm.2015.09.001)

Submitted on 31. May 2015, Revised on 22. August 2015, Accepted on 3. September 2015

Abstract

This paper presents a projection method for deriving membrane models from corresponding three-dimensional material models. As a particular example the anisotropic Holzapfel–Gasser–Ogden model is considered. The projection procedure is based on the kinematical and constitutive assumptions of general membrane theory, considering the membrane to be a general two-dimensional manifold. By assuming zero transverse stress, the Lagrange multiplier associated with the incompressibility constraint can be eliminated from the formulation. The resulting nonlinear model is discretized and linearized within the finite element method. Several numerical examples are shown, considering quadratic Lagrange and NURBS finite elements. These show that the proposed model is in very good agreement with analytical solutions and with full 3D finite element computations.

Keywords: anisotropic hyperelasticity, constitutive modeling, differential geometry, membrane theory, nonlinear finite elements, soft tissues

1 Introduction

Soft tissues are biological materials that are usually considered incompressible or nearly incompressible. They can easily undergo large deformations and therefore they show highly nonlinear behavior. Many living tissues are constructed from a ground substance of elastin reinforced by a network of collagen fibers. Examples of such materials are cardiovascular, lung and skin tissue (Fung, 1993). For such tissues, it is assumed that the ground matrix is isotropic while the distribution of collagen fibers exhibits anisotropic behavior (Holzapfel et al., 2000). Thus, any material model for soft biological tissues should take into account the geometrical and material nonlinearities as well as the anisotropic response. As many biological structures are geometrically thin, and are weak in bending and transverse shear deformation, they can be described within the framework of membrane theory. Within the human body, aneurysms, cell membranes, the mesentery, the meninges covering the brain and spinal chord, the pericardia around the heart, the visceral pleura supporting the lungs, skin, blood vessels, the urinary bladder, and fetal membranes are examples of biological membranes (Humphrey, 1998). Therefore, it is of great importance to develop a nonlinear membrane formulations that are not only able to

¹corresponding author, email: sauer@aices.rwth-aachen.de

²This pdf is the personal version of an article whose final publication is available at www.sciencedirect.com

treat the previously described challenges of biological membranes, but are also computationally efficient.

Although membrane theory and anisotropic hyperelasticity have been interesting subjects in the literature for quite some time, there are few studies that focus on nonlinear bio-membranes or rubber-like incompressible anisotropic membranes. The research in this area is mostly concerned with transversely isotropic hyperelasticity, which assumes that there is only one family of fibers, and orthotropic anisotropic hyperelastic membranes, which have two sets of identical orthogonal fibers. [Kyriacou et al. \(1996\)](#) proposed a finite element model for nonlinear orthotropic hyperelastic membranes derived from two-dimensional constitutive laws. [Humphrey \(1998\)](#) presented a theoretical framework to study nonlinear biological membranes. [Holzapfel et al. \(1996a\)](#) developed an isotropic membrane model that was modified by including the anisotropy of the material for axisymmetric membranes in [Holzapfel et al. \(1996b\)](#). [Reese et al. \(2001\)](#) introduced an orthotropic model to describe the behavior of pneumatic membranes reinforced with fibers. In [Kazakevičiūtė-Makovska \(2001\)](#), different nonlinear response functions for transversely isotropic elastic membranes were derived under conditions of incompressibility and plane stress. A challenge in the modeling of membranes is the phenomenon of wrinkling. The geometrical, mathematical and physical description of wrinkling is well studied ([Cerdea et al., 2002](#); [Cerdea and Mahadevan, 2003](#); [Puntel et al., 2011](#); [Taylor et al., 2014](#)). In particular, [Wu \(1978\)](#); [Steigmann and Pipkin \(1989\)](#); [Haseganu and Steigmann \(1994\)](#); [Wong and Pellegrino \(2006\)](#); [Wang et al. \(2007\)](#) have analyzed different aspects of nonlinear membrane wrinkling by finite element methods. [Massabò and Gambarotta \(2006\)](#) studied the wrinkling of biological membranes, restricted to isotropic materials. Through inverse finite element analysis, [Kroon and Holzapfel \(2009\)](#) examined elastic properties of anisotropic vascular membranes. [Borri-Brunetto et al. \(2009\)](#) analyzed response of a fibrous membrane based on the statistical distribution of the activation stretch of the collagen fibers. [Abdessalem et al. \(2011\)](#) developed a finite element model for orthotropic and transversely isotropic incompressible hyperelastic membranes. [Fan and Sacks \(2014\)](#) studied planar soft tissues using a structural constitutive model that distinguishes between fiber and ensemble strains. [Prot et al. \(2007\)](#) and [Tepole et al. \(2015\)](#) employed the anisotropic material model proposed by [Holzapfel et al. \(2000\)](#) to construct biological shell models. [Balzani et al. \(2010, 2008\)](#) analyzed anisotropic polyconvex energy densities for shells. For the particular case of biological membranes, the effect of residual stresses is studied e.g. by [Rausch and Kuhl \(2013\)](#) and [Balzani et al. \(2007\)](#).

Based on a new approach, in this paper, the anisotropic material model proposed by [Gasser et al. \(2006\)](#) is projected to a two-dimensional manifold within the framework of the nonlinear membrane formulation of [Sauer et al. \(2014\)](#). It should be noted, that the resulting model is a pure membrane, which mechanically is defined as a structure without bending stiffness. Membranes in the biophysical sense sometimes have considerable bending stiffness, and are therefore mechanical shells. In principle the procedure considered here can be extended to shells. A few remarks on this are given in [Sec. 2](#). This paper is organized in six sections. In the next section, the membrane theory, including the kinematics, strong and weak form of the membrane, is briefly reviewed. The three-dimensional and projected membrane models are introduced in [Sec. 3](#), followed by finite element discretization in [Sec. 4](#). Different numerical examples are then illustrated in [Sec. 5](#). The paper concludes with [Sec. 6](#).

2 Membrane theory

The large strain theory of membranes can be derived from nonlinear shell theories by neglecting the stresses associated with bending and transverse shear deformations (see e.g. [Kraus \(1967\)](#);

Libai (1988); Green (1992); Oden (2006)). It can also be derived from three-dimensional nonlinear elasticity (e.g. Steigmann (2009)). Nonlinear formulations of membranes, particularly for rubber-like material, have been studied in the past (see e.g. Oden and Sato (1967); Haughton and Ogden (1978); Fried (1982); Wriggers and Taylor (1990); Ibrahimbegovic and Gruttmann (1993); Bonet et al. (2000)). In this research, the computational membrane formulation developed by Sauer et al. (2014) is employed. The theory is formulated in the framework of curvilinear coordinates following Steigmann (1999). The considered membrane formulation is based on the following constitutive and kinematical assumptions: the resistance to bending is negligible, cross-sections remain planar during deformation, out-of-plane shear deformations are neglected and the thickness stretch is considered constant across the surface. As a consequence, the in-plane stresses of membrane are constant over the thickness. Therefore stresses can be directly derived from the strain energy density function of a two-dimensional manifold. More details can be found e.g. in Libai (1988); Green (1992). Furthermore, in order to avoid wrinkling, membranes are only studied under tension here.

2.1 Kinematics of membrane

In this section, the kinematics of nonlinear membranes in the framework of curvilinear coordinates is briefly summarized. For a detailed discussion of the membrane kinematics in curvilinear coordinates see for example Sauer et al. (2014) and Sauer (2014). The objective of this research is to project three-dimensional material models onto two-dimensional manifolds. Therefore the quantities that are needed to characterize the membrane kinematics are presented from a three-dimensional perspective. As earlier mentioned, in membrane theory, it is assumed that the membrane thickness is negligible compared to its other dimensions, even if it is curved, such that it can be treated as a surface. Furthermore, it should be noted that contrary to shells, out-of-plane shear deformations are not accounted for in membrane kinematics, which simplifies both theory and numerics considerably.

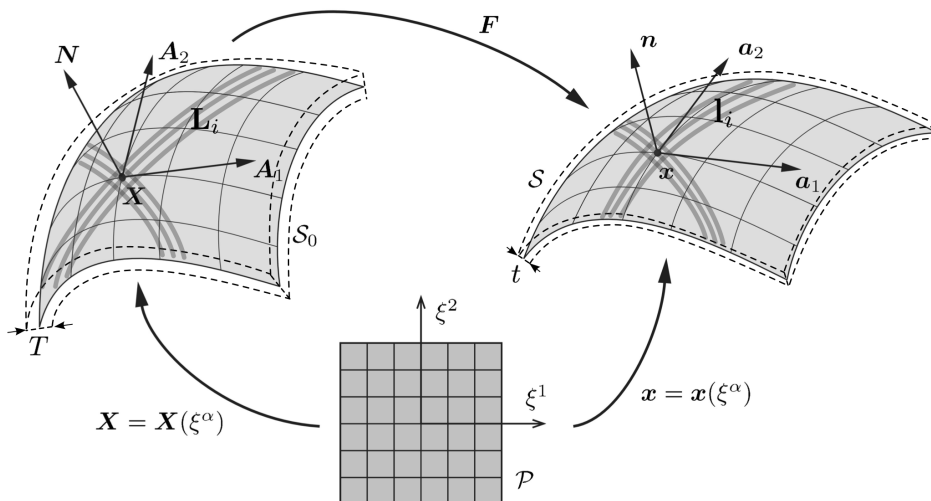


Figure 1: Mapping between parameter domain \mathcal{P} , reference surface \mathcal{S}_0 and current surface \mathcal{S} . The boundaries of the physical membrane are noted by dashed lines.

Membranes are thin structures that can be represented by two-dimensional manifolds. As shown

in Fig 1, the membrane initial mid-surface, denoted \mathcal{S}_0 , is fully characterized by the parametric description

$$\mathbf{X} = \mathbf{X}(\xi^1, \xi^2) . \quad (1)$$

This corresponds to a mapping of the point (ξ^1, ξ^2) in the parameter domain \mathcal{P} to the material point $\mathbf{X} \in \mathcal{S}_0$. The corresponding point on the deformed surface is

$$\mathbf{x} = \mathbf{x}(\xi^1, \xi^2) . \quad (2)$$

In the following, Greek letters are used to denote the two indices 1 and 2 for quantities on the membrane surface, and summation is implied on repeated indices. Furthermore, three-dimensional variables are distinguished by tilde and variables in reference and current configurations are denoted by uppercase and lowercase letters, respectively.

The tangent vectors to coordinate ξ^α at point $\mathbf{X} \in \mathcal{S}_0$ are given by

$$\mathbf{A}_\alpha = \frac{\partial \mathbf{X}}{\partial \xi^\alpha} , \quad \alpha = 1, 2 \quad (3)$$

and correspondingly

$$\mathbf{a}_\alpha = \frac{\partial \mathbf{x}}{\partial \xi^\alpha} . \quad (4)$$

As described in [Wriggers \(2008\)](#), the deformation gradient is represented in terms of the in-plane deformation gradient, \mathbf{F} , and the out-of-plane stretch, λ_3 as

$$\tilde{\mathbf{F}} = \mathbf{F} + \lambda_3 \mathbf{n} \otimes \mathbf{N} , \quad (5)$$

where \mathbf{F} is defined in terms of the tangent vectors of curvilinear coordinate system as

$$\mathbf{F} = \mathbf{a}_\alpha \otimes \mathbf{A}^\alpha . \quad (6)$$

The volume and area changes are given by the determinants of the three-dimensional and the in-plane deformation gradient as³

$$\tilde{J} = \det \tilde{\mathbf{F}} = J \lambda_3 , \quad (7)$$

$$J = \det \mathbf{F} = \sqrt{\det a_{\alpha\beta}} . \quad (8)$$

The right Cauchy-Green deformation tensor becomes

$$\tilde{\mathbf{C}} = \tilde{\mathbf{F}}^T \tilde{\mathbf{F}} = \mathbf{C} + \lambda_3^2 \mathbf{N} \otimes \mathbf{N} , \quad (9)$$

where

$$\mathbf{C} = \mathbf{F}^T \mathbf{F} = a_{\alpha\beta} \mathbf{A}^\alpha \otimes \mathbf{A}^\beta . \quad (10)$$

Consequently, the first invariants of the three-dimensional and the in-plane right Cauchy-Green deformation tensors are related by

$$\tilde{I}_1 = \tilde{\mathbf{C}} : \mathbf{I} = I_1 + \lambda_3^2 , \quad (11)$$

$$I_1 = \mathbf{C} : \mathbf{1}_0 = A^{\alpha\beta} a_{\alpha\beta} , \quad (12)$$

where \mathbf{I} and $\mathbf{1}_0$ are the three-dimensional and the reference in-plane identity tensors, respectively, which are related by

$$\mathbf{1}_0 := \mathbf{A}_\alpha \otimes \mathbf{A}^\alpha = \mathbf{A}^\alpha \otimes \mathbf{A}_\alpha = \delta_\alpha^\beta \mathbf{A}^\alpha \otimes \mathbf{A}_\beta = \mathbf{I} - \mathbf{N} \otimes \mathbf{N} . \quad (13)$$

³It should be noted that $\det \mathbf{F}$ is strictly defined in the tangent space as it would be zero otherwise.

The second and third invariants of the right Cauchy-Green deformation tensor are then

$$\tilde{I}_2 = \lambda_3^2 \tilde{\mathbf{C}} : \mathbf{I} + \det \mathbf{C} = \lambda_3^2 I_1 + J^2 , \quad (14)$$

$$\tilde{I}_3 = \lambda_3^2 \det \mathbf{C} = \lambda_3^2 J^2 . \quad (15)$$

Remark 1: As mentioned before, the presented theory considers pure membranes. Those have no bending stiffness. Some biological membranes, like lipid bilayers (Deseri et al., 2008; Deseri and Zurlo, 2013; Maleki et al., 2013; Steigmann, 2013; Deserno, 2015), can have considerable bending stiffness and should therefore be described by shell theory. In order to extend the present theory to shells, the bending resistance needs to be taken into account. Furthermore, the kinematical description needs to be generalized. For shells, the in-plane part of the deformation gradient of Eq. (6) is typically written as

$$\mathbf{F} = \mathbf{g}_\alpha \otimes \mathbf{G}^\alpha , \quad (16)$$

where \mathbf{g}_α and $\mathbf{G}^\alpha = G^{\alpha\beta} \mathbf{G}_\beta$ account for the different stretches across the thickness of the shell. See Wriggers (2008) and Sauer and Duong (2015) for details.

Remark 2: For membranes, two incompressibility constraints can be considered: area-incompressibility ($J = 1$) and classical bulk-incompressibility ($\tilde{J} = 1$) of the membrane material. The two are only identical if $\lambda_3 = 1$. For shells the deformation is not constant through the thickness, and one can therefore, in principle, choose a layer where to impose area-incompressibility.

2.2 Membrane strong form

The strong form equilibrium equation is obtained from the balance of linear momentum⁴ as

$$\mathbf{t}_{;\alpha}^\alpha + \mathbf{f} = \mathbf{0} . \quad (17)$$

Here \mathbf{f} is a distributed surface force, that can be decomposed as

$$\mathbf{f} = f_\alpha \mathbf{a}^\alpha + p \mathbf{n} = f^\alpha \mathbf{a}_\alpha + p \mathbf{n} , \quad (18)$$

where f_α and f^α are the co-variant and contra-variant in-plane components of \mathbf{f} , and p is the out-of-plane pressure acting on \mathcal{S} . According to Cauchy's formula

$$\mathbf{t}^\alpha = \boldsymbol{\sigma} \mathbf{a}^\alpha . \quad (19)$$

In general, the stress tensor takes the form

$$\boldsymbol{\sigma} = \sigma^{\alpha\beta} \mathbf{a}_\alpha \otimes \mathbf{a}_\beta + \sigma^{3\alpha} (\mathbf{n} \otimes \mathbf{a}_\alpha + \mathbf{a}_\alpha \otimes \mathbf{n}) + \sigma^{33} \mathbf{n} \otimes \mathbf{n} . \quad (20)$$

For membranes it is assumed that $\sigma^{3\alpha} = \sigma^{33} = 0$, so that

$$\boldsymbol{\sigma} = \sigma^{\alpha\beta} \mathbf{a}_\alpha \otimes \mathbf{a}_\beta . \quad (21)$$

Thus, the equilibrium Eq. (17) can be decomposed into

$$\begin{aligned} \sigma^{\beta\alpha}_{;\alpha} + f^\beta &= 0 , & (\text{in-plane equilibrium}), \\ \sigma^{\alpha\beta} b_{\alpha\beta} + p &= 0 , & (\text{out-of-plane equilibrium}). \end{aligned} \quad (22)$$

where $b_{\alpha\beta}$ are the co-variant components of the curvature tensor \mathbf{b} .

⁴In curvilinear coordinate systems, it is necessary to distinguish between the co-variant derivative (denoted by semicolon) and parametric derivative (denoted by comma). More details can be found e.g. in Kreyszig (1991).

2.3 Membrane weak form

As shown by [Sauer et al. \(2014\)](#), having the strong form of governing equation in Sec. (2.2), the corresponding weak form can be derived as

$$G_{\text{int}} - G_{\text{ext}} = 0 \quad \forall \mathbf{w} \in \mathcal{W} , \quad (23)$$

where

$$G_{\text{int}} := \int_{S_0} \mathbf{w}_{;\alpha} \cdot \boldsymbol{\tau}^{\alpha\beta} \mathbf{a}_\beta \, dA , \quad (24)$$

$$G_{\text{ext}} := \int_S w_\alpha f^\alpha \, da + \int_{\partial_t S} w_\alpha \bar{t}^\alpha \, ds + \int_S w p \, da , \quad (25)$$

and the Kirchhoff stress tensor $\boldsymbol{\tau} := J\boldsymbol{\sigma}$ is introduced. The weak form Eq. (23) is closed by Dirichlet and Neumann boundary conditions

$$\begin{aligned} \mathbf{u} &= \bar{\mathbf{u}} && \text{on } \partial_u S \\ \mathbf{t} &= \bar{\mathbf{t}} && \text{on } \partial_t S , \end{aligned} \quad (26)$$

where the prescribed displacement $\bar{\mathbf{u}}$ acts on the Dirichlet boundary condition and the prescribed boundary traction $\bar{\mathbf{t}} = \bar{t}^\alpha \mathbf{a}_\alpha$ is applied on the Neumann boundary $\partial_t S$.

3 Projection of three-dimensional constitutive relations

In this section, the procedure to project three-dimensional constitutive relations onto a two-dimensional manifold is explained. First, in Sec. (3.1), an anisotropic three-dimensional hyperelastic model suitable for soft tissues is introduced, and then a two-dimensional membrane version is derived in Sec. (3.2).

3.1 Three-dimensional anisotropic hyperelastic model

Here, an anisotropic hyperelastic material constitution is considered, which is used to model soft tissues with distributed collagen fiber orientations – in particular cardiovascular arteries. In the literature, it is usually called *HGO* model after being firstly introduced by [Holzapfel et al. \(2000\)](#). The model was later modified by [Gasser et al. \(2006\)](#) to include the dispersion of collagen fibers. For arterial layers with distributed collagen fibers, [Gasser et al. \(2006\)](#) proposed a strain energy function that depends only on three invariants, $\tilde{\Psi}_{\text{HGO}} = \tilde{\Psi}_{\text{HGO}}(\tilde{I}_1, \tilde{I}_4, \tilde{I}_6)$. Additionally, [Gasser et al. \(2006\)](#) assumed that $\tilde{\Psi}$ can be split into the isotropic response of the ground matrix, $\tilde{\Psi}_m$, and the anisotropic response of the fibers, $\tilde{\Psi}_f$. To impose the near incompressibility of the material, [Gasser et al. \(2006\)](#) decomposed the strain energy density function into a purely volumetric (*dilatational*) and a purely volume-preserving (*isochoric*) part.

Here, it is assumed that the material is fully incompressible, i.e. $\tilde{J} = 1$. In an approach that is different from the volumetric decomposition of [Gasser et al. \(2006\)](#), the incompressibility constraint,

$$g := 1 - \tilde{J} = 0 , \quad (27)$$

is included into the energy function by the Lagrange multiplier method (see e.g. [Sauer et al. \(2014\)](#)) such that the considered strain energy function becomes ([Holzapfel, 2004](#))

$$\tilde{\Psi}(\tilde{I}_1, \tilde{J}_1, \tilde{J}_2) = \tilde{\Psi}_m(\tilde{I}_1) + \tilde{\Psi}_f(\tilde{J}_1, \tilde{J}_2) + qg \quad (28)$$

with

$$\begin{aligned}\tilde{\Psi}_m &= \frac{\tilde{\mu}}{2}(\tilde{I}_1 - 3) \\ \tilde{\Psi}_f &= \tilde{\Psi}_f(\tilde{J}_1) + \tilde{\Psi}_f(\tilde{J}_2) = \frac{\tilde{k}_1}{2k_2} \sum_{i=1}^2 \{ \exp [k_2 (\tilde{J}_i - 1)^2] - 1 \},\end{aligned}\tag{29}$$

where \tilde{k}_1 is a stress-like parameter (with units kPa) and k_2 is a dimensionless parameter used to express the hyperelastic strain energy of two families of collagen fibers, which both should be obtained from mechanical tests of the tissue, and

$$\begin{aligned}\tilde{J}_1 &:= \tilde{I}_4 \\ \tilde{J}_2 &:= \tilde{I}_6\end{aligned}\tag{30}$$

are the fourth and sixth invariants determining the response of two families of collagen fibers with principle directions \mathbf{L}_1 and \mathbf{L}_2 in the reference configurations. From these the generalized structure tensors (*GST*)

$$\mathbf{H}_i := \kappa \mathbf{I} + (1 - 3\kappa) \mathbf{L}_i \otimes \mathbf{L}_i, \quad i = 1, 2\tag{31}$$

are defined. Here κ is the parameter determining the degree of anisotropy: $\kappa = 0$ implies that all fibers in a considered family \mathbf{L}_i are perfectly aligned. $\kappa = 1/3$ means that the fiber distribution is isotropic. κ can be determined from histological data of the tissue, e.g. by looking at the distribution (dispersion) of the fiber families, or it can be considered just as phenomenological parameter.

By means of the generalized structural tensor, Eq.(31), invariant \tilde{J}_i can be computed by

$$\tilde{J}_i = \tilde{\mathbf{C}} : \mathbf{H}_i = \kappa \tilde{I}_1 + (1 - 3\kappa)(\tilde{\mathbf{C}} : \mathbf{L}_i \otimes \mathbf{L}_i).\tag{32}$$

Thus, the second Piola–Kirchhoff stress tensor becomes

$$\tilde{\mathbf{S}} = 2 \frac{\partial \tilde{\Psi}}{\partial \tilde{\mathbf{C}}} = \tilde{\mu} \mathbf{I} + 2\tilde{k}_1 \sum_{i=1}^2 (\tilde{J}_i - 1) \exp [k_2 (\tilde{J}_i - 1)^2] \mathbf{H}_i - q \tilde{J} \tilde{\mathbf{C}}^{-1}.\tag{33}$$

Remark 3: We note that in a more general setting, the anisotropic strain energy function can be written as

$$\begin{aligned}\tilde{\Psi}_f &= \tilde{\Psi}_f(\tilde{J}_1) + \tilde{\Psi}_f(\tilde{J}_2) \\ &= \sum_{i=1}^2 \frac{\tilde{k}_{1i}}{2k_{2i}} \{ \exp [k_{2i} (\tilde{J}_i - 1)^2] - 1 \},\end{aligned}\tag{34}$$

where $k_{11} = k_{12}$ and $k_{21} = k_{22}$ for orthotropic, either $k_{11} = 0$ or $k_{12} = 0$ for transversely isotropic and $k_{11} = k_{12} = 0$ for isotropic hyperelastic materials.

3.2 Two-dimensional hyperelastic model with distributed collagen fiber orientations

Now we are able to derive the corresponding membrane constitution. To get the anisotropic part of the strain energy density function, it is necessary to find the structural tensors in terms of membrane quantities. Assuming in-plane fibers, i.e. $\mathbf{L}_1 \cdot \mathbf{N} = \mathbf{L}_2 \cdot \mathbf{N} = 0$, the preferred directions \mathbf{L}_i are represented in local coordinates as

$$\mathbf{L}_i = L_i^\alpha \mathbf{A}_\alpha; \quad L_i^\alpha = \mathbf{L}_i \cdot \mathbf{A}^\alpha,\tag{35}$$

so that

$$\mathbf{L}_i \otimes \mathbf{L}_i = L_i^{\alpha\beta} \mathbf{A}_\alpha \otimes \mathbf{A}_\beta; \quad L_i^{\alpha\beta} = L_i^\alpha L_i^\beta, \quad (36)$$

and

$$\tilde{\mathbf{C}} : \mathbf{L}_i \otimes \mathbf{L}_i = a_{\alpha\beta} L_i^{\alpha\beta} =: \lambda_{\mathbf{L}_i}^2, \quad (37)$$

where $\lambda_{\mathbf{L}_i}$ is the stretch in the preferred direction \mathbf{L}_i . Therefore, we get

$$\tilde{J}_i(a_{\alpha\beta}, \lambda_3) = \kappa I_1 + \kappa \lambda_3^2 + (1 - 3\kappa) \lambda_{\mathbf{L}_i}^2. \quad (38)$$

For a membrane, the stored strain energy per reference volume can be defined in terms of the stored strain energy per reference area as

$$\Psi(\mathbf{X}; \mathbf{C}) := \int_{-T/2}^{T/2} \tilde{\Psi}(\mathbf{X}, \xi; \tilde{\mathbf{C}}) d\xi = T \tilde{\Psi}(\tilde{\mathbf{X}}; \tilde{\mathbf{C}}), \quad (39)$$

where, according to membrane theory, $\tilde{\Psi}$ is assumed to be constant over the membrane thickness in the reference configuration T and accordingly the membrane strain energy density function becomes

$$\Psi(a_{\alpha\beta}, \lambda_3) = T \tilde{\Psi}(\tilde{\mathbf{C}}). \quad (40)$$

Considering Eq. (40) and substituting J and I_1 into Eq. (28), we get the strain energy for the membrane

$$\Psi(a_{\alpha\beta}, \lambda_3) = T \tilde{\Psi}(\tilde{I}_1, \tilde{J}_1, \tilde{J}_2) = \Psi_m(a_{\alpha\beta}, \lambda_3) + \Psi_f(a_{\alpha\beta}, \lambda_3) + qg, \quad (41)$$

with

$$\begin{aligned} \Psi_m &= \frac{\mu}{2} (I_1 + \lambda_3^2 - 3), \\ \Psi_f &= \frac{k_1}{2k_2} \sum_{i=1}^2 \{ \exp [k_2 (J_i + \kappa \lambda_3^2 - 1)^2] - 1 \}, \\ g &= 1 - J\lambda_3, \end{aligned} \quad (42)$$

where $\mu := T \tilde{\mu}$, $k_1 := T \tilde{k}_1$ and

$$J_i = \kappa I_1 + (1 - 3\kappa) \lambda_{\mathbf{L}_i}^2; \quad \lambda_{\mathbf{L}_i}^2 = a_{\alpha\beta} L_i^{\alpha\beta}. \quad (43)$$

Since it is assumed that fibers do not contribute to the compression, they are only active during extension, i.e. if $J_i + \kappa \lambda_3^2 > 1$ ($i = 1, 2$).

Remark 4: It has been proven that the *HGO* model is inaccurate for materials with a large dispersion of fibers (Raghupathy and Barocas, 2009; Cortes et al., 2010; Pandolfi and Vasta, 2012). In this sense, instead of generalized structural tensors (*GST*) that are also used in the presented model, the anisotropic strain energy density function can be expressed by angular integration (*AI*) of the strain energy of individual fibers, as discussed e.g. by Cortes et al. (2010). Accordingly, the three-dimensional strain energy density function $\tilde{\Psi}_f$ that is constructed by angular integration is reduced to a two-dimensional quantity Ψ_f through Eq. (40), which is used to derive the in-plane membrane stresses by Eqs. (57) and (58). In a similar fashion, the contribution of fibers in compression can also be modified. As discussed by Holzapfel and Ogden (2015), individual fibers within a family of distributed fibers can be shortened, while the stretch in the mean direction of fibers is greater than one. In accordance with Gasser et al. (2006), in the presented model it is required that the fibers contribute only when they are extended and not compressed, strictly when $\tilde{J}_i = J_i + \kappa \lambda_3^2 > 1$ ($i = 1, 2$). This deficiency can be systematically improved by including the modifications of the three-dimensional setup into the two-dimensional model.

3.3 Variations

In this section, the variation of the strain energy function due to variations of the independent variables $a_{\alpha\beta}$ and λ_3 is calculated. For \tilde{J}_i , the variation becomes

$$\delta\tilde{J}_i = \frac{\partial\tilde{J}_i}{\partial a_{\alpha\beta}}\delta a_{\alpha\beta} + \frac{\partial\tilde{J}_i}{\partial\lambda_3}\delta\lambda_3, \quad (44)$$

where

$$\begin{aligned} \frac{\partial\tilde{J}_i}{\partial\lambda_3} &= 2\kappa\lambda_3, \\ \frac{\partial\tilde{J}_i}{\partial a_{\alpha\beta}} &= \kappa A^{\alpha\beta} + (1 - 3\kappa)L_i^{\alpha\beta}. \end{aligned} \quad (45)$$

For isotropic and anisotropic strain energy functions it can be found that

$$\delta\Psi_m = \frac{\partial\Psi_m}{\partial a_{\alpha\beta}}\delta a_{\alpha\beta} + \frac{\partial\Psi_m}{\partial\lambda_3}\delta\lambda_3, \quad (46)$$

where

$$\begin{aligned} \frac{\partial\Psi_m}{\partial\lambda_3} &= \mu\lambda_3 \\ \frac{\partial\Psi_m}{\partial a_{\alpha\beta}} &= \frac{\mu}{2}A^{\alpha\beta}, \end{aligned} \quad (47)$$

and

$$\delta\Psi_f = \frac{\partial\Psi_f}{\partial a_{\alpha\beta}}\delta a_{\alpha\beta} + \frac{\partial\Psi_f}{\partial\lambda_3}\delta\lambda_3, \quad (48)$$

where

$$\begin{aligned} \frac{\partial\Psi_f}{\partial\lambda_3} &= \sum_{i=1}^2 \frac{\partial\Psi_f(\tilde{J}_i)}{\partial\tilde{J}_i} \frac{\partial\tilde{J}_i}{\partial\lambda_3} = \sum_{i=1}^2 2E_i\kappa\lambda_3, \\ \frac{\partial\Psi_f}{\partial a_{\alpha\beta}} &= \sum_{i=1}^2 \frac{\partial\Psi_f(\tilde{J}_i)}{\partial\tilde{J}_i} \frac{\partial\tilde{J}_i}{\partial a_{\alpha\beta}} = \sum_{i=1}^2 E_i \left(\kappa A^{\alpha\beta} + (1 - 3\kappa)L_i^{\alpha\beta} \right). \end{aligned} \quad (49)$$

Here

$$E_i := \frac{\partial\Psi_f(\tilde{J}_i)}{\partial\tilde{J}_i} = k_1(\tilde{J}_i - 1) \exp[k_2(\tilde{J}_i - 1)^2]. \quad (50)$$

For the incompressibility constraint, we find

$$\delta g = \frac{\partial g}{\partial a_{\alpha\beta}}\delta a_{\alpha\beta} + \frac{\partial g}{\partial\lambda_3}\delta\lambda_3, \quad (51)$$

where

$$\begin{aligned} \frac{\partial g}{\partial\lambda_3} &= -J, \\ \frac{\partial g}{\partial a_{\alpha\beta}} &= -\frac{\lambda_3 J}{2} a^{\alpha\beta} = -\frac{1}{2} a^{\alpha\beta}. \end{aligned} \quad (52)$$

3.4 Constitutive relations

Following [Sauer et al. \(2014\)](#), the Lagrange multiplier q can be computed by setting the out-of-plane stress σ_{33} to 0. Namely in this case, $\tilde{J} = J \lambda_3 = 1$ is substituted into Eq. (38) to give

$$\tilde{J}_i = \kappa I_1 + \kappa/J^2 + (1 - 3\kappa)\lambda_{L_i}^2 \quad (53)$$

and the out of plane stress can be computed by

$$\tilde{\sigma}_{33} = \frac{1}{JT} \left[\frac{\partial \Psi}{\partial \lambda_3} + q \frac{\partial g}{\partial \lambda_3} \right] = 0, \quad (54)$$

with

$$\frac{\partial \Psi}{\partial \lambda_3} = \frac{\partial \Psi_m}{\partial \lambda_3} + \frac{\partial \Psi_f}{\partial \lambda_3}. \quad (55)$$

From Eqs. (47), (49), (52), we find

$$q = \frac{1}{J^2} \left[\mu + 2\kappa \sum_{i=1}^2 E_i \right], \quad (56)$$

and the in-plane stress is computed by

$$\tau^{\alpha\beta} = 2 \left[\frac{\partial \Psi}{\partial a_{\alpha\beta}} + q \frac{\partial g}{\partial a_{\alpha\beta}} \right], \quad (57)$$

with

$$\frac{\partial \Psi}{\partial a_{\alpha\beta}} = \frac{\partial \Psi_m}{\partial a_{\alpha\beta}} + \frac{\partial \Psi_f}{\partial a_{\alpha\beta}}. \quad (58)$$

From Eqs. (47), (49), (52), and (56) we find

$$\begin{aligned} \tau^{\alpha\beta} &= \mu \left(A^{\alpha\beta} - \frac{a^{\alpha\beta}}{J^2} \right) + 2 \sum_{i=1}^2 E_i \left[\kappa \left(A^{\alpha\beta} - \frac{a^{\alpha\beta}}{J^2} \right) + (1 - 3\kappa)L_i^{\alpha\beta} \right] \\ &= \tau_m^{\alpha\beta} + \tau_f^{\alpha\beta}, \end{aligned} \quad (59)$$

where

$$\tau_m^{\alpha\beta} = \mu \left(A^{\alpha\beta} - \frac{a^{\alpha\beta}}{J^2} \right) \quad (60)$$

is the stress contribution from matrix material and

$$\tau_f^{\alpha\beta} = 2 \sum_{i=1}^2 E_i G_i^{\alpha\beta}, \quad (61)$$

$$G_i^{\alpha\beta} := \frac{\kappa}{\mu} \tau_m^{\alpha\beta} + (1 - 3\kappa)L_i^{\alpha\beta}, \quad (62)$$

is the stress contribution from fibers.

From Eq. (59), we find the symmetric elasticity tensor

$$c^{\alpha\beta\gamma\delta} := 2 \frac{\partial \tau^{\alpha\beta}}{\partial a_{\gamma\delta}} = 2 \frac{\mu}{J^2} \left[1 + 2 \frac{\kappa}{\mu} (E_1 + E_2) \right] (a^{\alpha\beta} a^{\gamma\delta} - a^{\alpha\beta\gamma\delta}) + 4 \sum_{i=1}^2 \alpha_i G_i^{\alpha\beta} G_i^{\gamma\delta}, \quad (63)$$

where

$$a^{\alpha\beta\gamma\delta} = -\frac{1}{2} \left(a^{\alpha\gamma} a^{\beta\delta} + a^{\alpha\delta} a^{\beta\gamma} \right), \quad (64)$$

$$\alpha_i := \left[k_1 + 2 k_1 k_2 (\tilde{J}_i - 1)^2 \right] \exp \left[k_2 (\tilde{J}_i - 1)^2 \right]. \quad (65)$$

4 Finite element discretization

The finite element method is used to solve the governing equation, Eq. (23), which is strongly nonlinear. By discretizing the initial surface \mathcal{S}_0 with a set of finite elements Ω_0^e , the deformation of the membrane is determined by the displacement of the nodal points \mathbf{X}_I of the reference configuration to position \mathbf{x}_I of the current configuration. Both quadratic Lagrange and NURBS elements are used for the finite element discretization.

4.1 FE interpolation

Considering a Bubnov-Galerkin formulation, both the deformation and the variation \mathbf{w} are approximated by the same interpolation functions, giving

$$\mathbf{X} \approx \mathbf{X}^h = \sum_I N_I \mathbf{X}_I = \mathbf{N} \mathbf{X}_e , \quad (66)$$

$$\mathbf{x} \approx \mathbf{x}^h = \sum_I N_I \mathbf{x}_I = \mathbf{N} \mathbf{x}_e , \quad (67)$$

$$\mathbf{a}_\alpha \approx \sum_I N_{I,\alpha} \mathbf{x}_I , \quad (68)$$

$$\mathbf{w} \approx \sum_I N_I \mathbf{w}_I = \mathbf{N} \mathbf{w}_e , \quad (69)$$

where $N_I = N_I(\xi^1, \xi^2)$ denotes the nodal shape function defined on the master element in parameter space, $N_{I,\alpha} = \partial N_I / \partial \xi^\alpha$ and $\mathbf{N} := [N_1 \mathbf{I}, \dots, N_I \mathbf{I}, \dots]$ is a $(3 \times 3n_{ne})$ array with the usual identity tensor \mathbf{I} and \mathbf{X}_e , \mathbf{x}_e , and \mathbf{w}_e are vectors containing the stacked nodal values for the element. Furthermore, w_α , w and $\mathbf{w}_{;\alpha}$ need to be approximated to find the discretize weak formulation. They follow as

$$\begin{aligned} w_\alpha &\approx \mathbf{w}_e^T \mathbf{N}^T \mathbf{N}_{,\alpha} \mathbf{x}_e , \\ w &\approx \mathbf{w}_e^T \mathbf{N}^T \mathbf{n} , \\ \mathbf{w}_{;\alpha} &\approx \mathbf{N}_{,\alpha} \mathbf{w}_e \end{aligned} \quad (70)$$

4.2 Discretized weak form

From Sauer et al. (2014), the discretized weak form, Eq. (23), can be represented in terms of FE force vectors,

$$\mathbf{w}^T [\mathbf{f}_{\text{int}} - \mathbf{f}_{\text{ext}}] = \mathbf{0} , \quad (71)$$

with

$$\mathbf{f}_{\text{ext}}^e = \int_{\Omega_0^e} \mathbf{N}^T \mathbf{f}_0 \, dA + \int_{\partial_t \Omega^e} \mathbf{N}^T \bar{\mathbf{t}} \, ds + \int_{\Omega^e} \mathbf{N}^T p \mathbf{n} \, da , \quad (72)$$

$$\mathbf{f}_{\text{int}}^e = \int_{\Omega_0^e} \mathbf{N}_{,\alpha}^T \tau^{\alpha\beta} \mathbf{N}_{,\beta} \, dA \mathbf{x}_e . \quad (73)$$

The solution of Eq. (23) is obtained by solving the nonlinear system of equations

$$\mathbf{f} := \mathbf{f}_{\text{int}} - \mathbf{f}_{\text{ext}} = \mathbf{0} , \quad (74)$$

apart from the nodes on the Dirichlet boundary.

4.3 FE linearization

The Newton–Raphson method is used to iteratively solve Eq. (74), which requires the linearization of Eq. (74). Both internal and external force vectors are linearized with respect to the nodal coordinates (see Sauer et al. (2014) for more details). We have

$$\Delta \mathbf{f}_{\text{int}}^e = \int_{\Omega_0^e} \mathbf{N}_{,\alpha}^T \Delta \tau^{\alpha\beta} \mathbf{N}_{,\beta} dA \mathbf{x}_e + \int_{\Omega_0^e} \mathbf{N}_{,\alpha}^T \tau^{\alpha\beta} \mathbf{N}_{,\beta} dA \Delta \mathbf{x}_e , \quad (75)$$

giving

$$\Delta \mathbf{f}_{\text{int}}^e = (\mathbf{k}_{\text{mat}}^e + \mathbf{k}_{\text{geo}}^e) \Delta \mathbf{x}_e , \quad (76)$$

with the stiffness matrices

$$\mathbf{k}_{\text{mat}}^e = \int_{\Omega_0^e} c^{\alpha\beta\gamma\delta} \mathbf{N}_{,\alpha}^T (\mathbf{a}_\beta \otimes \mathbf{a}_\gamma) \mathbf{N}_{,\delta} dA \quad (77)$$

and

$$\mathbf{k}_{\text{geo}}^e = \int_{\Omega_0^e} \mathbf{N}_{,\alpha}^T \tau^{\alpha\beta} \mathbf{N}_{,\beta} dA , \quad (78)$$

where $c^{\alpha\beta\gamma\delta}$ is calculated from Eq. (63). The linearized external force vector is

$$\Delta \mathbf{f}_{\text{ext}}^e = \int_{\Omega^e} \mathbf{N}^T \mathbf{n} \Delta p da + \int_{\Omega^e} \mathbf{N}^T p \Delta(\mathbf{n} da) , \quad (79)$$

where

$$\Delta \mathbf{f}_{\text{ext}}^e = \mathbf{k}_{\text{ext}}^e \Delta \mathbf{x}_e , \quad (80)$$

$$\mathbf{k}_{\text{ext}}^e = \int_{\Omega^e} \mathbf{N}^T \mathbf{n} \Delta p da + \int_{\Omega^e} p \mathbf{N}^T (\mathbf{n} \otimes \mathbf{a}^\alpha - \mathbf{a}^\alpha \otimes \mathbf{n}) \mathbf{N}_{,\alpha} da . \quad (81)$$

The presented projection method, which is based on curvilinear coordinate system and differential geometry, increases the numerical efficiency and facilitates the implementation as there is no need for mapping of derivatives between master and current (or reference) configuration. Furthermore, locally defined Cartesian bases are not required.

5 Numerical examples

In this section, several numerical examples are studied to investigate the accuracy and performance of the model. The inflation of a tube is considered and compared to the available analytical solution to examine the convergence of the proposed numerical scheme. Uniaxial stretching tests are compared with the results of the three-dimensional finite element analysis of Gasser et al. (2006). Finally, artery angioplasty is modeled through a contact problem to illustrate the performance of the proposed model in dealing with the numerical challenges of contact. The different material and geometrical parameters for each numerical example are listed in the Table 1.

Variable	Definition	Tube inflation	Uniaxial test	Angioplasty*
$\tilde{\mu}$	3D shear modulus [kN/m ²]	7.64	7.64	-
μ	2D shear modulus [N/m]	3.2852	3.82	7.64 T
\tilde{k}_1	Fibers 3D parameter [kN/m ²]	996.6	996.6	-
k_1	Fibers 2D parameter [N/m]	428.538	498.3	996.6/7.64 μ
k_2	Fibers dimensionless parameter	524.6	524.6	524.6
κ	Fibers dispersion parameter	0.0, 0.226, 1/3	0.0, 0.226	0.226
γ	Angle between fiber families [deg]	30, 40, 50	49.98	30
T	Membrane thickness [mm]	0.43	0.5	0.43 L_0
R	Tube radius [mm]	4.745	-	4.745 L_0
W	Specimen width [mm]	-	3	-
H	Specimen height [mm]	-	10	-

Table 1: List of parameters for different numerical examples. *For the angioplasty example, all parameters are dimensionless and normalized by the unit length L_0 and stress μ .

5.1 Tube inflation

In the first example, a thin tube with two identical families of collagen fibers is modeled. The problem geometry is shown in Fig. 2. The tube is inflated by applying the internal pressure p_i and the principle stresses and stretches are measured for comparison. The tube ends are set either free or pulled by an axial force. The two families of collagen fibers, with principal directions \mathbf{L}_1 and \mathbf{L}_2 , have the same mechanical properties and they are inclined equally from the axial direction, z . The inclination angle γ is measured from the tangential axis, θ , as shown in Fig. 2. Geometrical and mechanical quantities are extracted from Gasser et al. (2006). The derivation of the analytical solution for this problem is given in Appendix A.

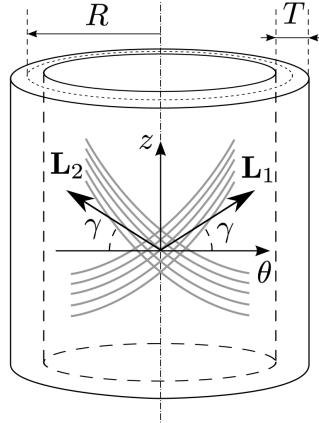


Figure 2: Geometry of thin tube model

On the tube ends, two different boundary conditions are considered, namely zero Dirichlet and zero Neumann boundary conditions. As the tube has three symmetry planes, the symmetry of the problem is used in order to model only 1/8 of the tube.

Fig. 3 shows the inflation of the tube with free ends. In this case, the traction on the tube ends is zero, i.e. $\bar{\sigma}_z = 0$, and the tube ends are free to move. As depicted in Fig. 3, three symmetry boundary conditions are applied on the corresponding edges. Quadratic Lagrange elements are used for meshing. The material and geometrical parameters are listed in Table 1. As shown in

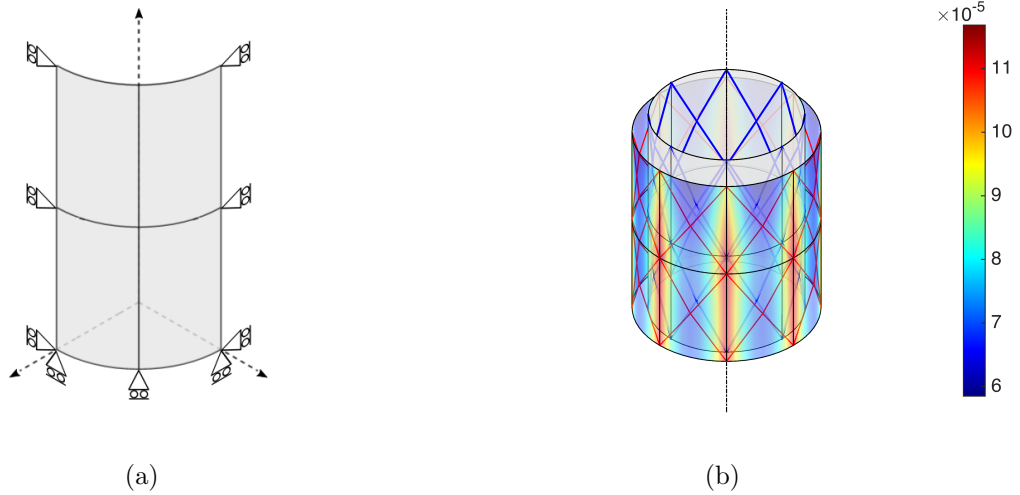


Figure 3: Zero Neumann BC: (a) undeformed configuration with BCs. (b) Deformed configuration coloured with relative error of λ_r (showing the full tube).

Figs. 4 and 5, the membrane model is able to accurately predict the stretches and stresses of the analytical solution. In Fig. 4, the relative error in the radial stretch $\lambda_r = 1/(\lambda_z \lambda_\theta)$ is plotted against the mesh size, which shows the desired convergence to the reference solution. The same trend is also observed for the axial and tangential stretches and corresponding stresses. The plotted error is the relative error of λ_r defined as

$$e(\lambda_r) = \frac{\sum_I^N |\lambda_r^I - \lambda_r^a|}{N \lambda_r^a}, \quad (82)$$

where λ_r^I is the computed radial stretch of the node I , λ_r^a is the radial stretch based on the analytical solution and N is the number of nodes. As it can be observed in Fig. 4, $e(\lambda_r) \sim N^{-2}$. Thus, the mesh refinement leads to quadratic convergence as it can be expected.

As illustrated in Fig. 5, the results of the FE analysis (denoted by circles) are in agreement with the analytical solution (denoted by lines). Three different dispersion parameters κ are considered with $\gamma = 30, 45$ and 60 deg. As it can be expected, if the fiber distribution is isotropic, i.e. $\kappa = 1/3$, the artery response does not change as γ varies.

A similar experiment is performed on a tube with fixed ends, i.e. zero Dirichlet boundary condition, as illustrated in Fig. 6. The material and geometrical parameters are the same as in the previous example. As it is shown in Fig. 6, in this case, the tube extension in axial direction is restricted, i.e. $\lambda_z = 1$. In addition to the radial stretches, the relative error in the axial reaction force F_z^S exerted on the tube end supports is also computed, as

$$e(F_z) = \frac{\sum_S^{N_s} |F_z^S - F_z^a|}{N F_z^a}, \quad (83)$$

where F_z^S is the computed axial reaction force of the support node S , F_z^a is the reaction force calculated analytically and N_s is the number of support nodes. As it is shown in Fig. 7, similar to the tube with Neumann boundary condition, the desired convergence is also observed here. In Fig. 8, the computed stretches and stresses in the axial and circumferential directions are compared with the analytical solution for different parameters.

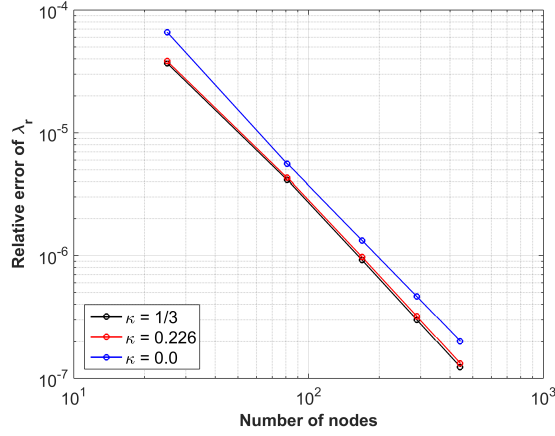


Figure 4: Zero Neumann BC: Convergence behavior of the relative error of λ_r vs. mesh size.

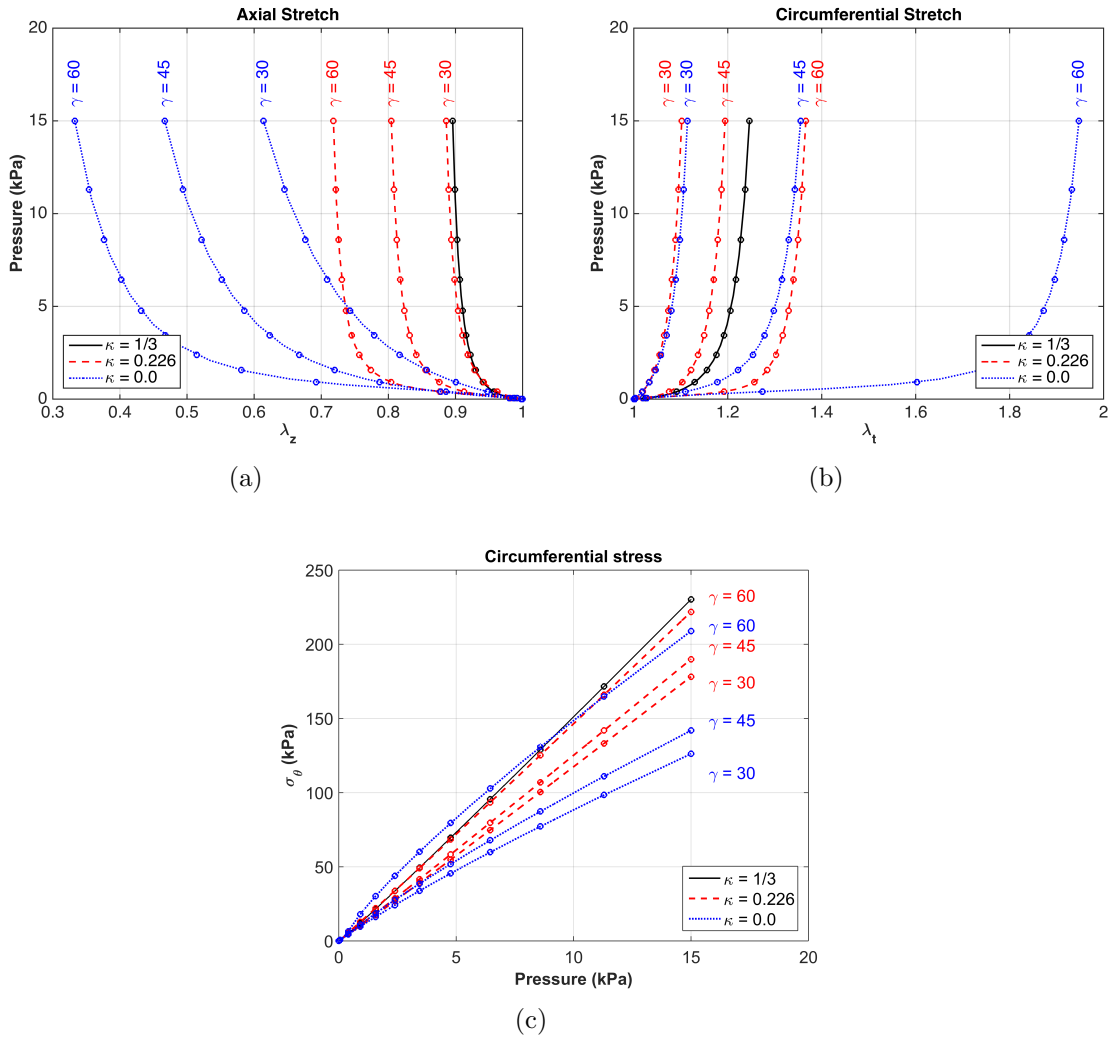


Figure 5: Zero Neumann BC: (a) axial stretches. (b) Circumferential stretches. (c) Circumferential stresses. Axial stresses are zero for both finite element and analytical approaches and are not plotted. The analytical solution is plotted with solid or dashed lines while FE results are denoted by circles

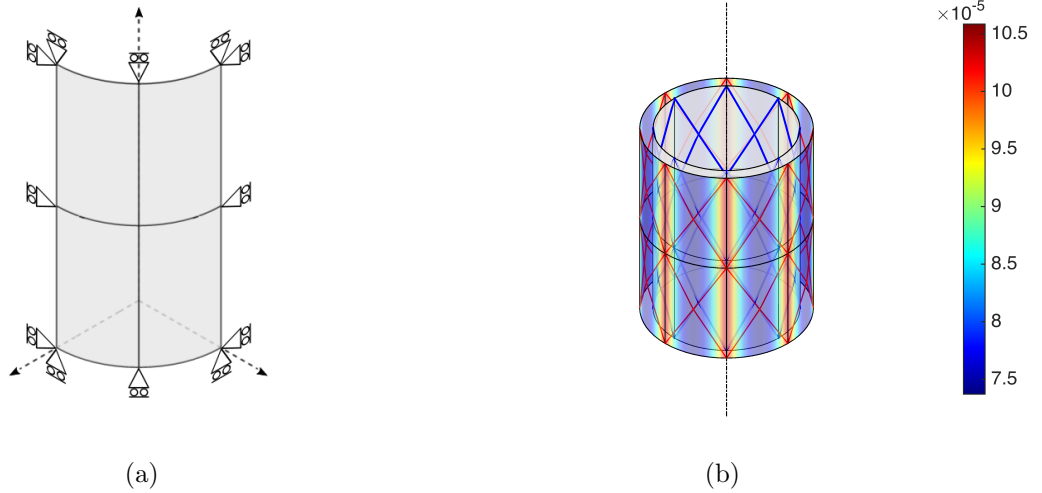


Figure 6: Zero Dirichlet BC: (a) Undeformed configuration with BCs. (b) Deformed configuration coloured with the relative error of λ_r (showing the full tube).

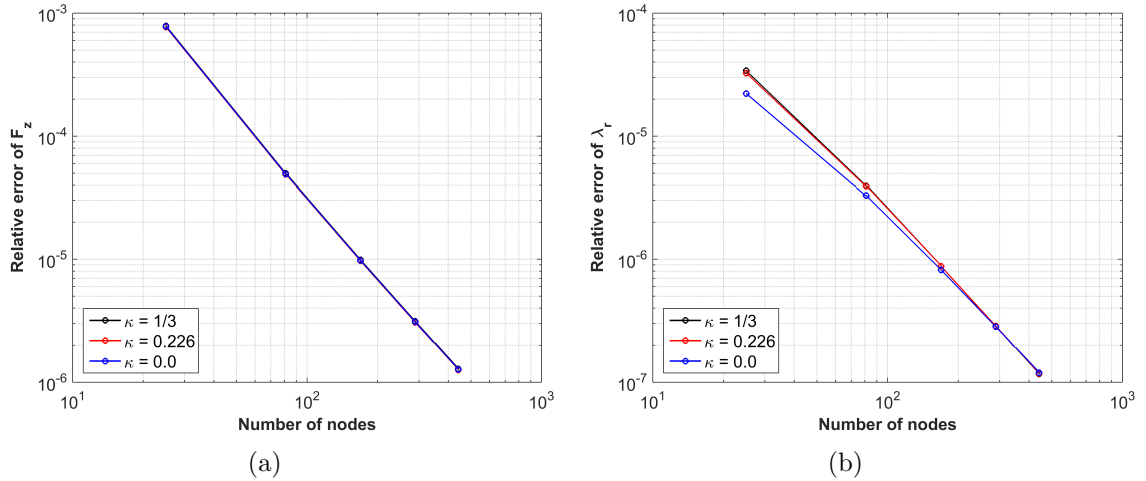


Figure 7: Zero Dirichlet BC: Convergence behavior of (a) the relative error of F_z (b) the relative error of λ_r vs. mesh size.

5.2 Uniaxial test

In this section, uniaxial tensile tests of membrane sheets are examined to show how close the proposed two-dimensional model gets to the three-dimensional model of Gasser et al. (2006). As schematically illustrated in Fig. 9, two circumferential and axial specimens are tested. Here it is assumed that the fiber angle $\gamma = 49.98$ deg. The other parameters can be found in Table 1. The circumferential and axial strains for ideal collagen fiber alignment ($\kappa = 0$) and dispersed collagen fiber ($\kappa = 0.226$) are shown in Fig. 9. The fiber orientation defined by parameter $c_l := (\mathbf{FL}_1) \cdot (\mathbf{FL}_2)$ is illustrated in Figs. 10 and 11 for $\kappa = 0$ and $\kappa = 0.226$, respectively. As it can be observed, both the 2D membrane model proposed here and the fully 3D model of Gasser et al. (2006) give very similar results. Here, 10×20 quadratic NURBS-based elements are used, which is computationally much cheaper than the reference model with 3200 hexahedral elements of Gasser et al. (2006). However, as the variation of sheet thickness is larger for $\kappa = 0.0$: a bigger difference is observed with respect to the three-dimensional result. The current thickness of the sheet is illustrated by the colored contour plot in Figs. 10c and 11c for $\kappa = 0.0$ and

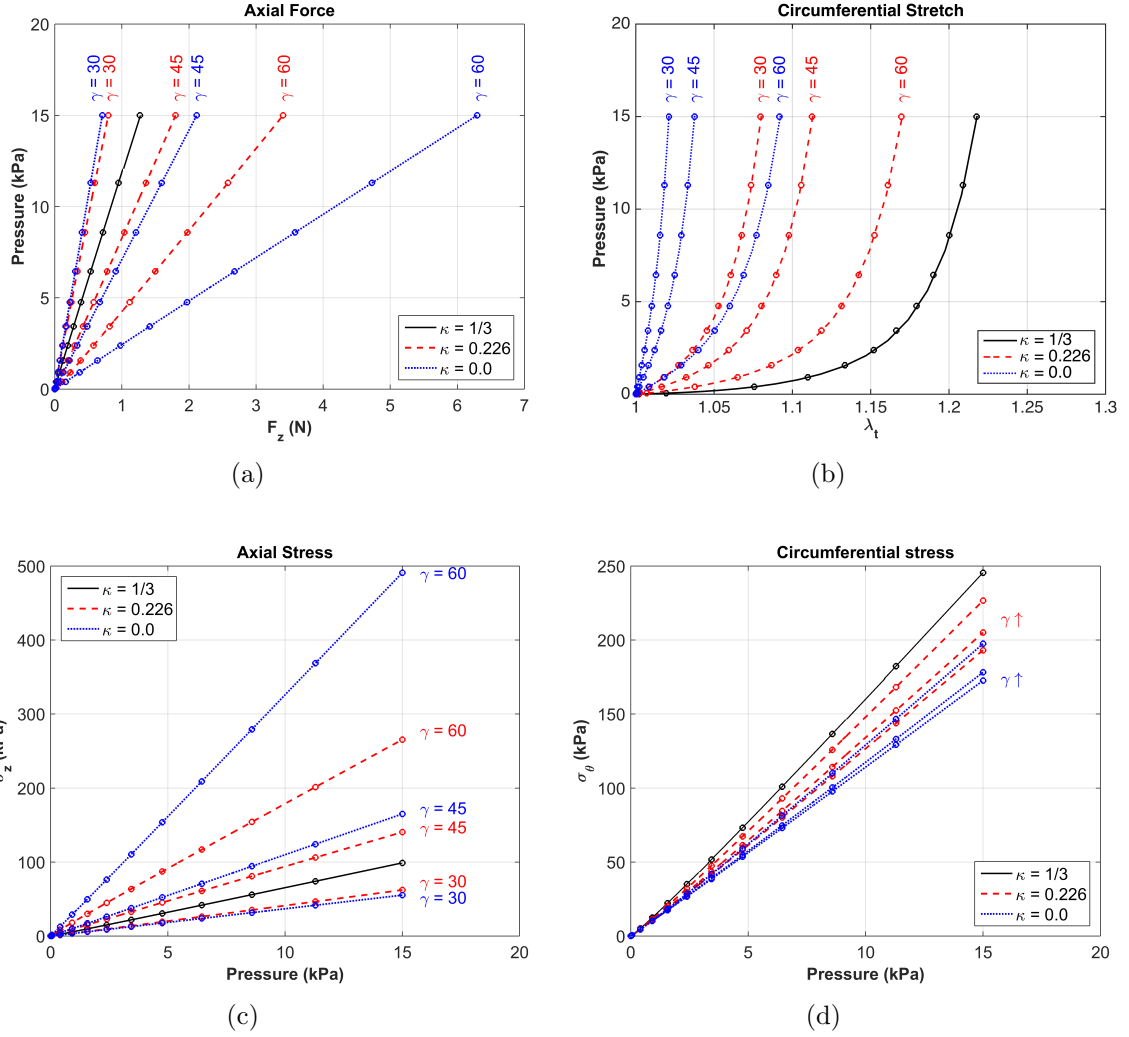


Figure 8: Zero Dirichlet BC: (a) axial force. (b) Circumferential stretches. (c) Axial stresses. (d) Circumferential stresses. The analytical solution is plotted with solid or dashed lines while FE results are denoted by circles

$\kappa = 0.226$, respectively.

5.3 Artery angioplasty

In this example, artery angioplasty is modeled. The artery wall with initial radius $R = 4.745 L_0$ and length $L = 12 L_0$ is first pre-stressed by the constant inner pressure $p = 0.1 \mu / L_0$ as is shown in Fig. 12. The ends of the artery wall are constrained by rigid diaphragms. A balloon with initial radius $R_b = 4.8 L_0$ is inflated so that it will contact the artery. The contact computations is based on an unbiased penalty formulation applied at the quadrature points of the isogeometric surface finite elements. All details of the formulation are given in Sauer and De Lorenzis (2015). The balloon is made of rubber with $\mu_b = 1000 \mu$ using the membrane model of Sauer et al. (2014). Here it is assumed that $\gamma = 30$ deg, $\kappa = 0.226$, $T = 0.43 L_0$, $\mu = 7.64 T$, $k_1 = 996.6 / 7.64 T$, $k_2 = 524.6$ and $L_0 = 1$. The penalty parameter for contact is $\epsilon = 1e4 \mu / L_0$. Both the balloon and the artery are discretized by quadratic NURBS with 8×8 elements. Due to the symmetry, only 1/8 of the model is used for the computation.

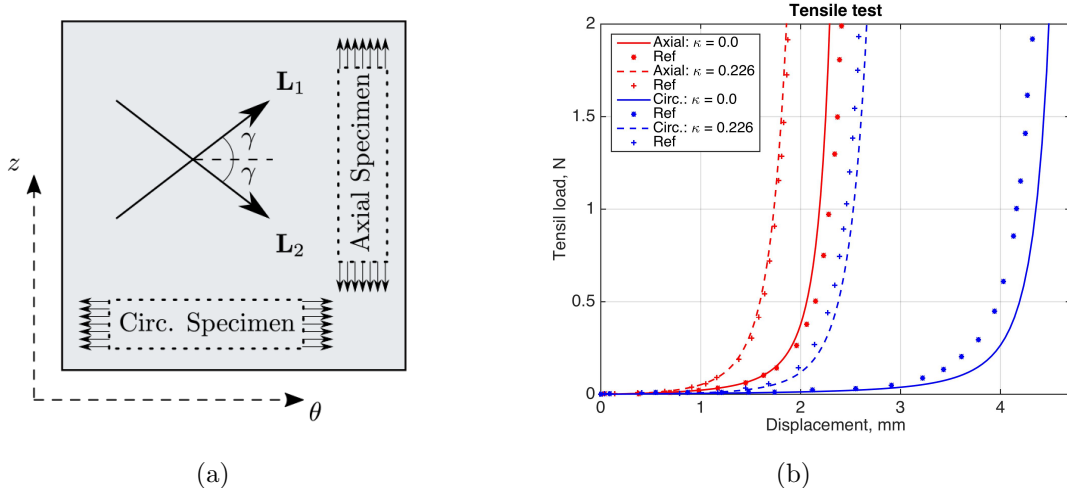


Figure 9: Tensile test of a sheet: (a) definition of axial and circumferential specimen. (b) The membrane solution, plotted by a line, is compared to the three-dimensional result of Gasser et al. (2006), denoted by circles.

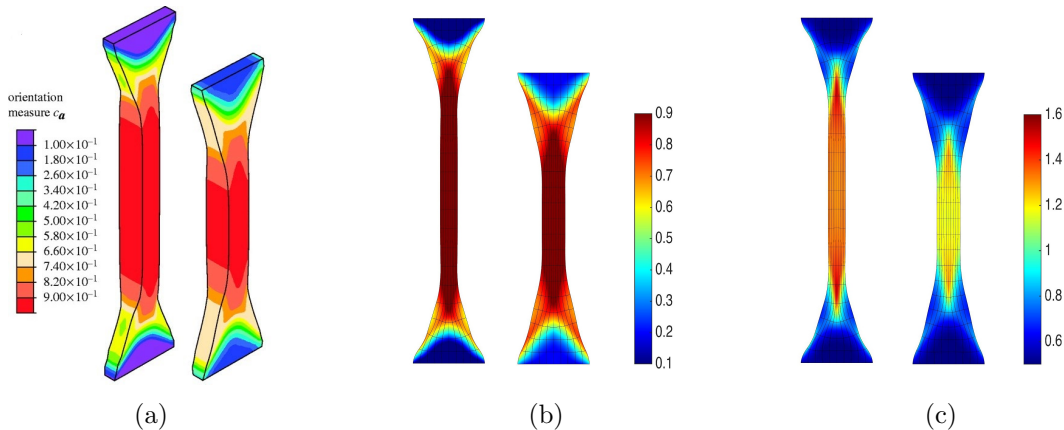


Figure 10: Uniaxial test at 1.0 N tensile load for $\kappa = 0$. (a) 3D finite element result of Gasser et al. (2006): fiber alignment $c_l := (\mathbf{F}\mathbf{L}_1) \cdot (\mathbf{F}\mathbf{L}_2)$ in circumferential (left) and axial direction (right) [adopted from the publisher website under CC BY 4.0 licence]. (b) Membrane setting: c_l in circumferential (left) and axial direction (right). (c) current thickness of the sheet $t = \lambda_3 T$ (mm) in circumferential (left) and axial direction (right).

6 Conclusion

In this study, a membrane formulation suitable for soft tissues with anisotropic incompressible hyperelastic material behavior is presented. The introduced model is a pure mathematical membrane and can be applied to biomembranes with negligible bending energy. A projection method is presented to reduce three-dimensional constitutive models to two-dimensional membrane formulations. In order to show the projection method, based on the general membrane model of Sauer et al. (2014), a constitutive model for incompressible anisotropic hyperelastic membranes is derived from the well-known three-dimensional anisotropic material model proposed by Gasser et al. (2006). This constitutive model is based on the decomposition of the strain energy function into isotropic and anisotropic components. The projection method, described in Sec. 3, can in principle also be adopted to other available three-dimensional biological material models.

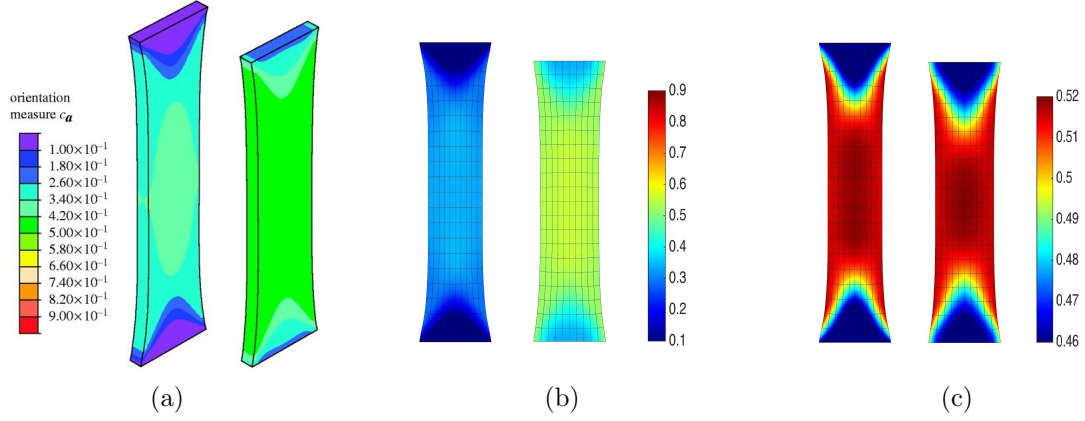


Figure 11: Uniaxial test at 1.0 N tensile load for $\kappa = 0.226$. (a) 3D finite element result of Gasser et al. (2006): fiber alignment $c_l := (\mathbf{F}\mathbf{L}_1) \cdot (\mathbf{F}\mathbf{L}_2)$ in circumferential (left) and axial direction (right) [adopted from the publisher website under CC BY 4.0 licence]. (b) Membrane setting: c_l in circumferential (left) and axial direction (right). (c) current thickness of the sheet $t = \lambda_3 T$ (mm) in circumferential (left) and axial direction (right).

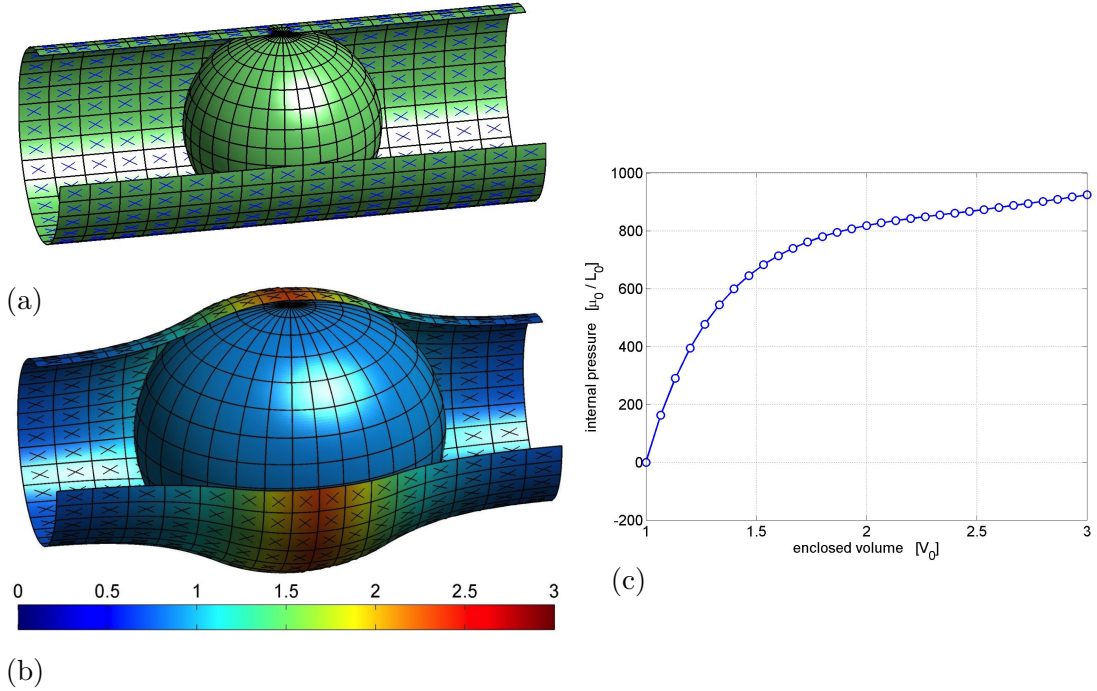


Figure 12: Artery angioplasty: (a) initial configuration: arterial wall is pre-stressed by $p = 0.1 \mu/L_0$ (the cross lines denote the fiber directions and the computational domain is mirrored). (b) Deformed configuration colored with $\bar{\gamma}_a = [\text{tr}(\boldsymbol{\tau}_m) + \text{tr}(\boldsymbol{\tau}_f)]/(2\mu)$ for the artery and $\bar{\gamma}_b = \text{tr}(\boldsymbol{\tau}_b)/(2\mu_b)$ for the balloon. (c) Volume–pressure curve.

The main benefit of the presented model is the considerable reduction in the number of degrees of freedom compared to the usual three-dimensional solid finite element discretization. As it is illustrated by various numerical examples, the membrane model can accurately predict the material response with a much lower computational cost compared to the existing models.

By illustrating different examples with both NURBS and Lagrange finite elements, the performance of the proposed formulation is evaluated. Results are in agreement with analytical

solutions and 3D finite element computations. As the theoretical formulation and numerical implementation show accurate results for the examined cases, it would be interesting to extend it to further examples, e.g. viscoelasticity and residual stresses. Additionally, the current projection formulation can be extended to shell formulation, which would be more realistic for thick biological structures like for example arteries.

Acknowledgment

Financial support from the German Research Foundation (DFG) through grant GSC 111, is gratefully acknowledged.

A Analytical solution of thin tube inflation

In this section, the deformation of a thin tube under uniform pressure is derived. First, the internal forces corresponding to Eq. (41) are obtained and then the external forces due to boundary tractions are found to close the problem. Denoting the strains in radial, circumferential and axial directions by λ_r , λ_θ and λ_z , respectively, in a cylindrical coordinate system, the deformation gradient and the right Cauchy-Green deformation tensors are

$$\tilde{\mathbf{F}} = \begin{bmatrix} \lambda_r & 0 & 0 \\ 0 & \lambda_\theta & 0 \\ 0 & 0 & \lambda_z \end{bmatrix}, \quad (84)$$

$$\tilde{\mathbf{C}} = \begin{bmatrix} \lambda_r^2 & 0 & 0 \\ 0 & \lambda_\theta^2 & 0 \\ 0 & 0 & \lambda_z^2 \end{bmatrix}, \quad (85)$$

Therefore, the first invariant of $\tilde{\mathbf{C}}$ is

$$\tilde{I}_1 = \tilde{\mathbf{C}} : \mathbf{I} = \lambda_r^2 + \lambda_\theta^2 + \lambda_z^2. \quad (86)$$

The fibers are structured as a helix so that the direction of fibers is $\mathbf{L}_i = [0, \cos \gamma, \sin \gamma]^T$. Thus, the fourth invariant is

$$\tilde{I}_4 = \tilde{\mathbf{C}} : \mathbf{L}_i \otimes \mathbf{L}_i = \lambda_\theta^2 \cos^2 \gamma + \lambda_z^2 \sin^2 \gamma. \quad (87)$$

For the given symmetric configuration, it can be shown that the stress field is

$$\tilde{\sigma}_r = \lambda_r \frac{\partial \tilde{\Psi}}{\partial \lambda_r}, \quad \tilde{\sigma}_\theta = \lambda_\theta \frac{\partial \tilde{\Psi}}{\partial \lambda_\theta}, \quad \tilde{\sigma}_z = \lambda_z \frac{\partial \tilde{\Psi}}{\partial \lambda_z}. \quad (88)$$

The strain energy density function is already derived in Eqs. (28) and (29). The determinant of the deformation gradient is $\tilde{J} = \lambda_r \lambda_\theta \lambda_z$ and the isotropic and anisotropic parts of the strain energy functions are

$$\tilde{\Psi}_m = \frac{\tilde{c}}{2} (\tilde{I}_1 - 1) \quad (89)$$

and

$$\tilde{\Psi}_f = \frac{k_1}{k_2} [\exp(k_2 E^2) - 1] \quad (90)$$

for two identical families of fibers with $E = \kappa \tilde{I}_1 + (1 - 3\kappa) \tilde{I}_4$.

A.1 Internal forces

To find the radial stress $\tilde{\sigma}_r$, the derivative of the strain energy function with respect to the radial strain is needed. We find

$$\frac{\partial \tilde{\Psi}_m}{\partial \lambda_r} = c \lambda_r , \quad (91)$$

$$\frac{\partial \tilde{\Psi}_f}{\partial \lambda_r} = 4 k_1 \kappa E \exp(k_2 E^2) \lambda_r , \quad (92)$$

$$\frac{\partial g}{\partial \lambda_r} = -\lambda_z \lambda_\theta = -\lambda_r^{-1} , \quad (93)$$

$$\tilde{\sigma}_r = [c + 4 k_1 \kappa E \exp(k_2 E^2)] \lambda_r^2 - q . \quad (94)$$

Assuming plane-stress conditions, $\tilde{\sigma}_r = 0$, the Lagrange multiplier for the incompressibility constraint is found as

$$q = [c + 4 k_1 \kappa E \exp(k_2 E^2)] \lambda_r^2 . \quad (95)$$

In a same fashion, the axial stress $\tilde{\sigma}_z$ is calculated as

$$\frac{\partial \tilde{\Psi}_m}{\partial \lambda_z} = c \lambda_z , \quad (96)$$

$$\frac{\partial \tilde{\Psi}_f}{\partial \lambda_z} = 4 k_1 (\kappa + (1 - 3 \kappa) \sin^2 \gamma) E \exp(k_2 E^2) \lambda_z , \quad (97)$$

$$\frac{\partial g}{\partial \lambda_r} = -\lambda_r \lambda_\theta = -\lambda_z^{-1} , \quad (98)$$

Therefore

$$\tilde{\sigma}_z = (c + \kappa D) [\lambda_z^2 - (\lambda_z \lambda_\theta)^{-2}] + (1 - 3 \kappa) D \sin^2 \gamma \lambda_z^2 , \quad (99)$$

where

$$D = 4 k_1 E \exp(k_2 E^2) . \quad (100)$$

and similarly for the circumferential stress,

$$\tilde{\sigma}_\theta = (c + \kappa D) [\lambda_t^2 - (\lambda_z \lambda_\theta)^{-2}] + (1 - 3 \kappa) D \cos^2 \gamma \lambda_t^2 . \quad (101)$$

A.2 External forces

If the radius and the thickness of the tube in the reference configuration are R and T , respectively, the corresponding quantities in the deformed configuration are

$$\begin{aligned} r &= \lambda_\theta R , \\ t &= \lambda_r T = (\lambda_z \lambda_\theta)^{-1} T . \end{aligned} \quad (102)$$

As shown in Fig. 13, assuming that the internal pressure of tube is p_i , the circumferential (hoop) stress is

$$\bar{\sigma}_\theta = \frac{p_i r}{t} = \frac{p_i R}{T} \lambda_\theta^2 \lambda_z . \quad (103)$$

If the tube ends are free, $\bar{\sigma}_z = 0$, if the tube ends are fixed, i.e. $\lambda_z = 1$ then $\bar{\sigma}_z = \tilde{\sigma}_z(1, \lambda_\theta)$ and if the tube ends are pulled, e.g. the tube is closed, $\bar{\sigma}_z$ is obtained by force balance

$$\bar{\sigma}_z (2 \pi r t) = p_i (\pi r^2) + F , \quad (104)$$

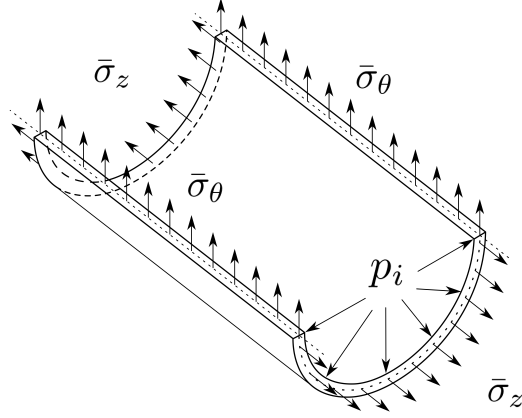


Figure 13: Thin tube boundary tractions

where F is the external force applied on the tube ends and therefore

$$\begin{aligned}\bar{\sigma}_z &= \frac{p_i r}{2 t} + \frac{F}{2 \pi r t} \\ &= \frac{p_i R}{2T} \lambda_\theta^2 \lambda_z + \frac{F}{2 \pi R T} \lambda_z .\end{aligned}\tag{105}$$

A.3 Solution

The deformed configuration is found by solving the following system of nonlinear equations, which is constructed by the balance of external and internal forces.

$$\begin{aligned}f_1(\lambda_z, \lambda_\theta) &:= \tilde{\sigma}_\theta - \bar{\sigma}_\theta = 0 \\ f_2(\lambda_z, \lambda_\theta) &:= \tilde{\sigma}_z - \bar{\sigma}_z = 0\end{aligned}\tag{106}$$

Due to the nonlinearity of the equations, they are solved numerically by an iterative method like the Newton–Raphson method. If Dirichlet boundary conditions are applied on tube ends, i.e. the tube ends are fixed, only the first equation needs to be solved. Eq. (106) is solved iteratively through

$$\mathbf{K} \Delta \mathbf{\Lambda} = \mathbf{f} ,\tag{107}$$

where

$$\mathbf{f} = \begin{bmatrix} f_1 \\ f_2 \end{bmatrix} ,\tag{108}$$

$$\mathbf{\Lambda} = \begin{bmatrix} \lambda_z \\ \lambda_\theta \end{bmatrix} ,\tag{109}$$

and

$$\mathbf{K} = \begin{bmatrix} \frac{\partial \tilde{\sigma}_\theta}{\partial \lambda_z} & \frac{\partial \tilde{\sigma}_\theta}{\partial \lambda_\theta} \\ \frac{\partial \tilde{\sigma}_z}{\partial \lambda_z} & \frac{\partial \tilde{\sigma}_z}{\partial \lambda_\theta} \end{bmatrix} - \begin{bmatrix} \frac{\partial \bar{\sigma}_\theta}{\partial \lambda_z} & \frac{\partial \bar{\sigma}_\theta}{\partial \lambda_\theta} \\ \frac{\partial \bar{\sigma}_z}{\partial \lambda_z} & \frac{\partial \bar{\sigma}_z}{\partial \lambda_\theta} \end{bmatrix} .\tag{110}$$

Here the linearized terms and elements of the tangent matrix are calculated as

$$E_z = \frac{\partial E}{\partial \lambda_z} = 2 \kappa (\lambda_z - \lambda_z^{-3} \lambda_\theta^{-2}) + 2 (1 - 3 \kappa) \sin^2 \gamma \lambda_z ,\tag{111}$$

$$E_\theta = \frac{\partial E}{\partial \lambda_\theta} = 2 \kappa (\lambda_\theta - \lambda_z^{-2} \lambda_\theta^{-3}) + 2 (1 - 3 \kappa) \cos^2 \gamma \lambda_\theta , \quad (112)$$

$$D_z = \frac{\partial D}{\partial \lambda_z} = 4 k_1 \exp(k_2 E^2) (1 + 2 k_2 E^2) E_z , \quad (113)$$

$$D_\theta = \frac{\partial D}{\partial \lambda_\theta} = 4 k_1 \exp(k_2 E^2) (1 + 2 k_2 E^2) E_\theta , \quad (114)$$

$$\begin{aligned} \frac{\partial \tilde{\sigma}_\theta}{\partial \lambda_z} &= 2 (c + \kappa D) \lambda_z^{-3} \lambda_\theta^{-2} \\ &+ \kappa D_z \left[\lambda_z^2 - (\lambda_z \lambda_\theta)^{-2} \right] + (1 - 3 \kappa) D_z \sin^2 \gamma \lambda_z^2 , \end{aligned} \quad (115)$$

$$\begin{aligned} \frac{\partial \tilde{\sigma}_\theta}{\partial \lambda_\theta} &= 2 (c + \kappa D) \left[\lambda_\theta + \lambda_z^{-2} \lambda_\theta^{-3} \right] + 2 (1 - 3 \kappa) D \cos^2 \gamma \lambda_\theta \\ &+ \kappa D_\theta \left[\lambda_z^2 - (\lambda_z \lambda_\theta)^{-2} \right] + (1 - 3 \kappa) D_\theta \cos^2 \gamma \lambda_\theta^2 , \end{aligned} \quad (116)$$

$$\begin{aligned} \frac{\partial \tilde{\sigma}_z}{\partial \lambda_z} &= 2 (c + \kappa D) \left[\lambda_z + \lambda_z^{-3} \lambda_\theta^{-2} \right] + 2 (1 - 3 \kappa) D \sin^2 \gamma \lambda_z \\ &+ \kappa D_z \left[\lambda_z^2 - (\lambda_z \lambda_\theta)^{-2} \right] + (1 - 3 \kappa) D_z \sin^2 \gamma \lambda_z^2 , \end{aligned} \quad (117)$$

$$\begin{aligned} \frac{\partial \tilde{\sigma}_z}{\partial \lambda_\theta} &= 2 (c + \kappa D) \lambda_z^{-2} \lambda_\theta^{-3} \\ &+ \kappa D_\theta \left[\lambda_z^2 - (\lambda_z \lambda_\theta)^{-2} \right] + (1 - 3 \kappa) D_\theta \sin^2 \gamma \lambda_z^2 , \end{aligned} \quad (118)$$

$$\frac{\partial \bar{\sigma}_\theta}{\partial \lambda_z} = \frac{p_i R}{T} \lambda_\theta^2 , \quad (119)$$

$$\frac{\partial \bar{\sigma}_\theta}{\partial \lambda_\theta} = 2 \frac{p_i R}{T} \lambda_\theta \lambda_z . \quad (120)$$

If $\bar{\sigma}_z = 0$, $\frac{\partial \bar{\sigma}_z}{\partial \lambda_z} = \frac{\partial \bar{\sigma}_z}{\partial \lambda_\theta} = 0$, otherwise

$$\frac{\partial \bar{\sigma}_z}{\partial \lambda_z} = \frac{p_i R}{2T} \lambda_\theta^2 + \frac{F}{2 \pi R T} , \quad (121)$$

$$\frac{\partial \bar{\sigma}_z}{\partial \lambda_\theta} = \frac{p_i R}{T} \lambda_\theta \lambda_z . \quad (122)$$

References

- Abdessalem, J., Kallel, I. K., and Fakhreddine, D. (2011). Theory and finite element implementation of orthotropic and transversely isotropic incompressible hyperelastic membrane. *Multidiscip. Model. Mater. Struct.*, **7**(4):424–439.
- Balzani, D., Gruttmann, F., and Schröder, J. (2008). Analysis of thin shells using anisotropic polyconvex energy densities. *Comput. Methods Appl. Mech. Eng.*, **197**(912):1015 – 1032.
- Balzani, D., Schröder, J., and Gross, D. (2007). Numerical simulation of residual stresses in arterial walls. *Comput. Mater. Sci.*, **39**:117–123.
- Balzani, D., Schröder, J., and Neff, P. (2010). Applications of anisotropic polyconvex energies: thin shells and biomechanics of arterial walls. In *Poly-, Quasi- and Rank-One Convexity in Applied Mechanics*, volume **516**, pages 131–176. Springer Vienna.

- Bonet, J., Wood, R. D., and Mahaney, J. (2000). Aspects of the analysis of membrane structures. In *Computational civil and structural engineering*, pages 105–113. Civil-Comp. Press.
- Borri-Brunetto, M., Chiaia, B., and Deambrosi, M. (2009). A micromechanical model for fibrous biological membranes at finite strain. *Biomater. Tissue Eng.*, **3**:1–23.
- Cerda, E. and Mahadevan, L. (2003). Geometry and physics of wrinkling. *Phys. Rev. Lett.*, **90**:074302.
- Cerda, E., Ravi-Chandar, K., and Mahadevan, L. (2002). Thin films: Wrinkling of an elastic sheet under tension. *Nature*, **419**(6907):579–580.
- Cortes, D., Lake, S., Kadlowec, J., Soslowsky, L., and Elliott, D. (2010). Characterizing the mechanical contribution of fiber angular distribution in connective tissue: comparison of two modeling approaches. *Biomech. Model. Mechanobiol.*, **9**(5):651–658.
- Deseri, L., Piccioni, M., and Zurlo, G. (2008). Derivation of a new free energy for biological membranes. *Contin. Mech. Thermodyn.*, **20**(5):255–273.
- Deseri, L. and Zurlo, G. (2013). The stretching elasticity of biomembranes determines their line tension and bending rigidity. *Biomech. Model. Mechanobiol.*, **12**(6):1233–1242.
- Deserno, M. (2015). Fluid lipid membranes: From differential geometry to curvature stresses. *Chem. Phys. Lipids*, **185**:11 – 45. (Membrane mechanochemistry: From the molecular to the cellular scale).
- Fan, R. and Sacks, M. S. (2014). Simulation of planar soft tissues using a structural constitutive model: Finite element implementation and validation. *J. Biomech.*, **47**(9):2043 – 2054. Functional Tissue Engineering.
- Fried, I. (1982). Finite element computation of large rubber membrane deformations. *Int. J. Numer. Mech. Engng.*, **18**:653–660.
- Fung, Y. C. (1993). *Biomechanics: Mechanical Properties of Living Tissues*. Springer-Verlag, New York.
- Gasser, T. C., Ogden, R. W., and Holzapfel, G. A. (2006). Hyperelastic modelling of arterial layers with distributed collagen fibre orientations. *J. R. Soc. Interface*, **3**:15–35.
- Green, A. E. (1992). *Theoretical elasticity*. Dover, New York.
- Haseganu, E. and Steigmann, D. (1994). Analysis of partly wrinkled membranes by the method of dynamic relaxation. *Comput. Mech.*, **14**(6):596–614.
- Haughton, D. and Ogden, R. (1978). On the incremental equations in non-linear elasticity — I. Membrane theory. *J. Mech. Phys. Solids*, **26**(2):93 – 110.
- Holzapfel, G. A. (2004). Computational biomechanics of soft biological tissue. In *Encyclopedia of computational mechanics*, pages 604–635. John Wiley & Sons, Ltd, Chichester, West Sussex, UK.
- Holzapfel, G. A., Eberlein, R., Wriggers, P., and Weizsäcker, H. W. (1996a). Large strain analysis of soft biological membranes: Formulation and finite element analysis. *Comput. Methods Appl. Mech. Eng.*, **132**(12):45 – 61.

- Holzapfel, G. A., Eberlein, R., Wriggers, P., and Weizsäcker, H. W. (1996b). A new axisymmetrical membrane element for anisotropic, finite strain analysis of arteries. *Commun. Numer. Methods Eng.*, **12**(8):507–517.
- Holzapfel, G. A., Gasser, T. C., and Ogden, R. W. (2000). A new constitutive framework for arterial wall mechanics and a comparative study of material models. *J. Elast. Phys. Sci. Solids*, **61**(1-3):1–48.
- Holzapfel, G. A. and Ogden, R. W. (2015). On the tension-compression switch in soft fibrous solids. *Eur. J. Mech. A:Solids*, **49**:561 – 569.
- Humphrey, J. D. (1998). Comput. methods membrane biomechanics. *Computer Methods Biomech. Biomed. Eng.*, **1**(3):171–210.
- Ibrahimbegovic, A. and Gruttmann, F. (1993). A consistent finite element formulation of nonlinear membrane shell theory with particular reference to elastic rubberlike material. *Finite Elem. Anal. Des.*, **13**(1):75–86.
- Kazakevičiūtė-Makovska, R. (2001). Non-linear response functions for transversely isotropic elastic membranes. *Statyba*, **7**(5):345–351.
- Kraus, H. (1967). *Thin elastic shells: an introduction to the theoretical foundations and the analysis of their static and dynamic behavior*. Wiley, New York.
- Kreyszig, E. (1991). *Differential Geometry*. Dover.
- Kroon, M. and Holzapfel, G. A. (2009). Elastic properties of anisotropic vascular membranes examined by inverse analysis. *Comput. Methods Appl. Mech. Eng.*, **198**(4546):3622 – 3632. Models and Methods in Computational Vascular and Cardiovascular Mechanics.
- Kyriacou, S., Humphrey, J., and Schwab, C. (1996). Finite element analysis of nonlinear orthotropic hyperelastic membranes. *Comput. Mech.*, **18**(4):269–278.
- Libai, A. (1988). *The Nonlinear Theory of Elastic Shells: One Spatial Dimension*. Academic Press, Boston.
- Maleki, M., Seguin, B., and Fried, E. (2013). Kinematics, material symmetry, and energy densities for lipid bilayers with spontaneous curvature. *Biomech. Model. Mechanobiol.*, **12**(5):997–1017.
- Massabò, R. and Gambarotta, L. (2006). Wrinkling of plane isotropic biological membranes. *J. Appl. Mech.*, **74**(3):550–559.
- Oden, J. T. (2006). *Finite Elements of Nonlinear Continua*. Dover Edition.
- Oden, J. T. and Sato, T. (1967). Finite strains and displacements of elastic membranes by the finite element method. *Int. J. Solids Struct.*, **3**(4):471–488.
- Pandolfi, A. and Vasta, M. (2012). Fiber distributed hyperelastic modeling of biological tissues. *Mech. Mater.*, **44**:151 – 162. Microstructures and Anisotropies.
- Prot, V., Skallerud, B., and Holzapfel, G. A. (2007). Transversely isotropic membrane shells with application to mitral valve mechanics. constitutive modelling and finite element implementation. *Int. J. Numer. Methods Eng.*, **71**(8):987–1008.
- Puntel, E., Deseri, L., and Fried, E. (2011). Wrinkling of a stretched thin sheet. *J. Elast.*, **105**(1-2):137–170.

- Raghupathy, R. and Barocas, V. H. (2009). A closed-form structural model of planar fibrous tissue mechanics. *J. Biomech.*, **42**(10):1424–1428.
- Rausch, M. K. and Kuhl, E. (2013). On the effect of prestrain and residual stress in thin biological membranes. *J. Mech. Phys. Solids*, **61**(9):1955 – 1969.
- Reese, S., Raible, T., and Wriggers, P. (2001). Finite element modelling of orthotropic material behaviour in pneumatic membranes. *Int. J. Solids Struct.*, **38**(52):9525 – 9544.
- Sauer, R. A. (2014). A contact theory for surface tension driven systems. *Math. Mech. Solids*, published online, DOI: 10.1177/1081286514521230.
- Sauer, R. A. and De Lorenzis, L. (2015). An unbiased computational contact formulation for 3D friction. *Inter. J. Numer. Methods Eng.*, **101**(4):251–280.
- Sauer, R. A. and Duong, T. X. (2015). On the theoretical foundations of thin solid and liquid shells. *Math. Mech. Solids*, published online, DOI: 10.1177/1081286515594656.
- Sauer, R. A., Duong, T. X., and Corbett, C. J. (2014). A computational formulation for constrained solid and liquid membranes considering isogeometric finite elements. *Comput. Methods Appl. Mech. Eng.*, **271**:48–68.
- Steigmann, D. (2009). A concise derivation of membrane theory from three-dimensional non-linear elasticity. *J. Elast.*, **97**(1):97–101.
- Steigmann, D. (2013). A model for lipid membranes with tilt and distension based on three-dimensional liquid crystal theory. *Inter. J. Non-Linear Mech.*, **56**:61 – 70. Soft Matter: a nonlinear continuum mechanics perspective.
- Steigmann, D. and Pipkin, A. (1989). Wrinkling of pressurized membranes. *ASME. J. Appl. Mech.*, **56**(3):624–628.
- Steigmann, D. J. (1999). On the relationship between the Cosserat and Kirchhoff-Love theories of elastic shells. *Math. Mech. Solids*, **4**:275–288.
- Taylor, M., Bertoldi, K., and Steigmann, D. J. (2014). Spatial resolution of wrinkle patterns in thin elastic sheets at finite strain. *J. Mech. Phys. Solids*, **62**:163 – 180.
- Tepole, A. B., Kabaria, H., Bletzinger, K.-U., and Kuhl, E. (2015). Isogeometric kirchhofflove shell formulations for biological membranes. *Comput. Methods Appl. Mech. Eng.*, **293**:328 – 347.
- Wang, C., Tan, H., Du, X., and Wan, Z. (2007). Wrinkling prediction of rectangular shell-membrane under transverse in-plane displacement. *Inter. J. Solids Struct.*, **44**(20):6507–6516.
- Wong, Y. and Pellegrino, S. (2006). Winkled membranes. Part 3: numerical simulations. *J. Mech. Mater. Struct.*, **1**:6395.
- Wriggers, P. (2008). *Nonlinear Finite Element Methods*. Springer.
- Wriggers, P. and Taylor, R. L. (1990). A fully non-linear axisymmetrical membrane element for rubber-like materials. *Engrg. Comput.*, **7**(1):303–310.
- Wu, C. (1978). Nonlinear wrinkling of nonlinear membranes of revolution. *ASME. J. Appl. Mech.*, **45**(3):533–538.